

Analysis of the Origins of κ (Kappa) to Compute Hard Rock to Rock Adjustment Factors for GMPEs

Chris Van Houtte and Stéphane Drouet* and Fabrice Cotton

ISTerre, Université Joseph Fourier, CNRS, BP 53, 38041 Grenoble Cedex 9, France

* Now at Geoter International, RN96 - Espace 890, 13360 Roquevaire, France

July 18, 2011

Abstract

The observable decay with frequency (f) of Fourier amplitude spectra for ground-motion recordings is controlled by a parameter κ : $\exp(-\pi\kappa f)$. We analyze data from the KIK-net network, which is composed of stations with paired ground-motion sensors, one at the surface and one in a borehole. This study estimates κ for all KIK-net stations, using earthquakes recorded between 1998 and 2006. An inversion scheme is used to separate site, source and path contributions to κ .

We correlate the site component of κ (κ_0), estimated at the surface and at depth, with different S-wave velocity measures and with the fundamental

resonant frequency of the site. The results show that the best correlations involve shallow soil S-wave velocity measures. The superficial layers of the soil predominantly influence κ_0 but a remaining component with a deep origin is also observed. The source component of κ is small and presents a clear regional dependence, while no correlations with magnitude or depth of the earthquake are observed.

Data from the NGA database are also used to estimate κ_0 (surface site component) at the stations with a measured V_{S30} value. The V_{S30} - κ couples estimated from both KIK-net and NGA data are compared with results from the literature and a new correlation is established.

Most of the Ground-Motion Prediction Equations (GMPEs) for stable continental regions are derived for very hard rock sites ($V_{S30} > 2000$ m/s). In order to use these equations for standard rock sites (V_{S30} around 800 m/s) conversion factors are required. Using the new correlation V_{S30} - κ and the host-to-target adjustment method of Campbell (2003), we compute amplification factors from very hard rock to rock. We show that in these conversions, the effect of both v_{S30} and κ have to be taken into account.

1 Introduction

The present study is motivated by 3 main objectives: 1) computing κ (the high-frequency decay) and analyzing its origin; 2) building a new V_{S30} - κ correlation; 3) using these results to compute very hard rock to rock site adjustment factors.

Describing the shape of the Fourier amplitude spectrum of ground mo-

tion recordings is very important for earthquake engineering purposes (e.g. McGuire, 1978).

The shape of the spectrum is well documented for low frequencies. Initially, the amplitudes increase at ω^2 (where $\omega = 2\pi f$) until a corner frequency, f_0 (Aki, 1967; Brune, 1970). Beyond the corner frequency, the shape of the spectrum has been characterized differently. Some studies have suggested that above the corner frequency, the spectrum is flat up to a cut-off frequency, f_{max} (Hanks, 1982), above which the spectrum rapidly decays as (Boore, 1983):

$$\left[1 + (f/f_{max})^8\right] \quad (1)$$

An alternative model (Anderson and Hough, 1984) characterized the shape of the spectrum at high frequencies as exponentially decaying, given by:

$$a(f) = A_0 \exp(-\pi\kappa f) \text{ for } f > f_E \quad (2)$$

where f_E is a frequency above which the decay is approximately linear on a plot of $\log[a(f)]$ against f , A_0 is a source and propagation path dependent amplitude and κ (“kappa”) is a spectral decay parameter controlling the rate of amplitude fall-off with frequency. This study focuses on the Anderson and Hough (1984) model for high-frequency decay, with no further attention being paid to the f_{max} -dependent model.

Despite κ being a commonly-accepted parameter for representing the behaviour of Fourier spectra at high frequencies, the mechanism causing this observed fall-off has been heavily debated. Some suggest that the attenuation arises from a site effect in the near-surface material (Hanks, 1982),

while others prefer a source-dependency, where the source doesn't produce high frequencies due to fault non-elasticity (Papageorgiou and Aki, 1983). Anderson and Hough (1984) found that κ increases with epicentral distance r , which is consistent with the effect of anelastic attenuation:

$$\exp\left(-\frac{\pi r f}{Q v_S}\right) \quad (3)$$

where r is the distance, Q the quality factor and v_S the S-wave velocity.

More recently, it has been suggested that the high-cut process is a combination of all three, source, distance and site, with distance having the least significance of the three (Tsai and Chen, 2000).

To obtain a more meaningful parameter, the distance-dependence can be eliminated by extrapolating the $\kappa(r)$ trend to $r=0$, introducing another parameter at the intercept, κ_0 . κ_0 denotes the site attenuation a few kilometers immediately beneath the station (Hough *et al.*, 1988). κ_0 has become an accepted and commonly applied high-frequency filter parameter. However, there is still no consensus as to its origin, an understanding of which is required before it can be applied to ground motion prediction and seismic hazard analyses.

An analysis by Silva and Darragh (1995) showed that near-surface attenuation (modeled through κ_0) predominantly influences response spectra content for frequencies greater than about 5-10Hz. Average κ_0 values of 0.037 s were determined for Western North America (WNA) and 0.008 s for Eastern North America (ENA). This analysis clearly documents the difference in rock spectral content in WNA and ENA as reflected in the factor of

3 to 4 difference in κ_0 .

The first objective of this study is to use the unique KIK-net data to re-examine the high frequency attenuation debate that began 30 years ago, using the κ_0 parameter described above. κ_0 at both the surface and at depth is checked against various source- or site-specific parameters to find potential dependencies. The KIK-net network from Japan, provides data unavailable to previous studies, with twin sensors installed at the surface and at depth. The borehole data then provides a unique opportunity to better understand the mechanism of high-frequency spectral fall-off (i.e. the origin of κ_0), because the contribution of the superficial material between the two sensors can be isolated.

The second objective of this study is to refine the correlation between V_{S30} (the average shear wave velocity in the uppermost 30 meters) and κ_0 . This correlation is a key relation used for host-to-target adjustments of empirical Ground-Motion Prediction Equations (GMPEs) (e.g. Cotton *et al.*, 2006; Bommer *et al.*, 2010). Although it has been questioned whether V_{S30} is a relevant parameter for describing the subsurface structure (Castellaro *et al.*, 2008), it is still used as a basis for site classifications in seismic codes worldwide. Moreover, as site specific κ_0 's are usually not available (because of the lack of records), ground-motion prediction of such sites, defined only by geotechnical parameters like V_{S30} , then depends on available correlations between V_{S30} and κ_0 . Previous attempts have been made (Silva *et al.*, 1998; Chandler *et al.*, 2006; Drouet *et al.*, 2010) to obtain a meaningful correlation between V_{S30} and κ_0 , however this study hopes to validate and strengthen this correlation using surface recordings from both the KIK-net and NGA

databases. The NGA database does not provide borehole recordings, so is only applicable to the second aim of this study. However, it does provide further validation with the KIK-net results, and those from previous κ_0 - V_{S30} correlation.

GMPEs for crustal earthquakes are split in two main categories: equations for active crustal regions and for stable continental regions. It is not always evident which type of equation to use, especially in regions of low to moderate seismicity like Western Europe. Equations for stable continental regions are defined for very hard rock conditions ($V_{S30} > 2000$ m/s) while the equations for active crustal regions are valid for rock sites with V_{S30} around 800 m/s. Consequently, some adjustments are needed to homogenize the ground-motion predictions using both sets of equations. Our third objective is to use our updated correlation between V_{S30} and κ_0 to determine properties of generic hard rock and rock sites and to refine the amplification factors between the two types of rock sites. Using the host-to-target adjustment method (Campbell, 2003), we convert ground-motion predictions for very hard rock sites condition to rock site condition based on two GMPEs: Toro *et al.* (1997) and Campbell (2003).

2 Data

The first and main dataset that is employed in this study is the Kiban-Kyoshin network (KIK-net). Located in Japan, KIK-net has two sensors installed at each station. One of the sensors is positioned at the surface, with the other usually installed at a depth of either 100 (GL-100) or 200 (GL-

200) meters below ground surface (Fujiwara *et al.*, 2004). Each instrument is a three-component accelerograph with a 24 bit analog-to-digital converter, using a 200 Hz sampling frequency. The stations retained for this study are shown in Figure 1 with the events recorded between 1998 and 2006. The magnitude-distance scatter and the depth distribution of the events are also shown in Figure 1. This study utilises both borehole and surface recordings from the selected stations. Detailed velocity profiles are available at most stations, determined from downhole loggings (Fujiwara *et al.*, 2004). Cadet *et al.* (2010) compiled station information: average S-wave velocities over various depth (5, 10, 20, 30 meters); S-wave velocities below the downhole sensor; and average S-waves velocities between the surface and downhole sensors. They also determined the resonant frequency of the surface site from H/V earthquakes measurements (see Table S1 available as an electronic supplement to this paper).

The Next Generation of Attenuation (NGA) database is a collection of high quality strong ground motion recordings from around the world, although most of the records are from California and Taiwan (Chiou *et al.*, 2008). We retained the stations for which a measured V_{S30} value was available (see Table S2 available as an electronic supplement to this paper), neglecting those for which V_{S30} was only estimated. The selected dataset is shown in Figure 2. As this study considers regionally dependent parameters, only the Californian and Taiwanese records were analyzed, to ensure sufficiently large regional datasets.

In order to select stations located either on stiff soil or rock, we kept in the analysis only the stations with measured V_{S30} (at the surface) greater than

500 m/s (the stations in Figure 1 and Figure 2 fulfil that criterion). The overall advantages of the KIK-net and NGA datasets are that the stations are densely spaced, the data are digitised (most of them for NGA), accurate V_{S30} are available and the dataset is of unprecedented volume and quality. The details for the number of earthquakes, stations and records for the two datasets are given in Table 1. As will be shown later, the data sets for shallow events (depth ≤ 25 km) and deep events (depth > 25 km) give different results in terms of attenuation with distance, therefore they are not merged in this analysis.

3 Method

All the Fourier spectra analyzed here are computed solely from the S-wave portion of the recordings. P- and S-wave arrival times were manually picked. Picking of the S-wave time-window was standardised, by using the portion of the recording starting at the S-wave onset and ending where 80% of the total energy was recorded. According to Tsai and Chen (2000) the window length has very little influence on the determination of κ , as long as the strong energetic part of S-waves is encapsulated in the selected window. Each record was visually examined to ensure that the correct part of the time series was selected. The picks were generally satisfactory, except in some recordings, where multiple ruptures occurred. Such records were discarded from the analysis (the numbers in Table 1 do not include such data).

As defined by Anderson and Hough (1984), κ should be calculated using the linear least-squares fit to the spectra at high frequencies (in frequency/log-

amplitude space). Slopes were manually picked, up to a maximum frequency, defined for Japan as the smallest of: the frequency at which the level of noise exceeds the signal; or 50 Hz, above which we consider the spectra unreliable (half the Nyquist frequency). For the NGA data, we relied on the frequency band indicated in the metadata file (<http://peer.berkeley.edu/nga/flatfile.html>). The frequency at which the spectra starts to decrease linearly with frequency (f_E) was visually estimated and is varying between 1-2 Hz to 10-20 Hz depending on the record. Dividing the values of the slope by $-\pi$ gives a value for κ .

In general, the borehole recordings exhibit an obvious linear decay at high frequencies (Fig. 3), allowing the slopes to be easily and accurately picked. However, with most surface recordings, site amplification effects leave spikes in the spectra, making it more difficult to pick the slope. The undue influence from site effects can bias the picking, leading to erroneously high values of κ (Parolai and Bindi, 2004). We made some tests to correct the spectra for the site effect using H/V from earthquakes, SSR (standard spectral ratio using the borehole sensor as reference), or theoretical site amplifications computed from the given velocity profiles for the Japanese data (Fig. 4). However, it turned out that although the correction removed part of the resonant frequency amplifications, the high frequency part of the site amplification function was not well defined and the correction was introducing problems at high frequencies. Consequently we decided to keep the original spectra for further analysis. The site effect might bias the estimation of κ , and this can explain the higher variability we observed for surface κ s compared to downhole κ s (as shown in the following).

To isolate the distance-dependence of κ , stations were separated into regions, where the propagation paths of seismic waves would be similar. For the KIK-net Stations from Japan, we separated recordings from shallow and deep events, while the Taiwanese and Californian stations from the NGA database were also separated. For each region, κ is plotted against hypocentral distance, r , (Figure 5). For the KIK-net data, only borehole κ s are used to define regional attenuation, as they are less affected by site effects than the surface κ s are. This ensures that the distance term is better resolved.

For the NGA data, all the computed κ values for each record at an individual station are extrapolated along the regional $\kappa(r)$ trend to $r=0$, using the regional average distance dependence, and the average of these $\kappa(0)$ values is a station-specific κ_0 . Performing this process for all stations gives a surface κ_0 for each station.

Taking advantage of the large amount of KIK-net data, we set up an inversion procedure following Purvance and Anderson (2003) aiming at the decomposition of κ into a source, a site and a propagation component:

$$\kappa(r) = \kappa_{source} + \kappa_{0-downhole} + \kappa_{0-surface} + slope \times r \quad (4)$$

Such a formulation implies a degree of freedom, which is resolved using the assumption that the average source component of κ is 0, as proposed by Purvance and Anderson (2003):

$$\sum_{number\ of\ sources} \kappa_{source} = 0 \quad (5)$$

As a consequence, the absolute values of the source component of κ have no meaning, but the relative values from event to event do.

The sheer volume of KIK-net data greatly improves the quality of the results. It allows us to neglect records or stations of insufficient quality from the analysis, while maintaining an adequately large dataset. Only records that complied with the following performance criteria were included in the analysis: at a single station, the difference between the values of κ on the two horizontal components should be less than 25%; and the borehole κ should be less than the surface κ . Moreover, for the inversion process we only kept the events recorded by at least 3 stations and the stations that recorded at least 3 events.

4 Results

Figure 5 illustrates the distance-dependence of κ for Japan at depth and at the surface for shallow (depth < 25 km mostly crustal) and deep (depth ≥ 25 km mostly subduction zone) events, and the distance-dependence of κ at the surface for California and Taiwan. Spectral decay clearly increases with hypocentral distance. Regional variations of the slope are observed, which are probably linked with regional attenuation properties (i.e., the quality factor). The decay is also different for crustal and subduction zone events for which the waves travel through materials with different properties. There is also less variability for the borehole records than for the surface records, confirming that the site effects may bias the estimation of κ .

For the KIK-net data, the deep events were excluded from the inversion,

since the propagation properties differ from those for shallow events (Figure 5). Some tests were carried out on the parameterization of κ . Three different hypotheses have been chosen: 1) κ only depends on the site; 2) κ only depends on the source; 3) κ includes both site and source dependencies. Additionally, the distance dependence of κ is tested in each of the above-mentioned cases. Note that the distance term is estimated from only downhole records to avoid site amplifications which could bias the distance term. Table 2 shows the variances of the residuals of those tests. In order to check that the distributions of residuals have physically different variances, we performed the F-test as shown in Table 2. An F-test value much greater or much smaller than 1, associated with low F-test probability, indicates that the distributions have different variances. As shown by Table 2, the model leading to the smallest variance is the last one, with a site, a source, and a distance dependence of κ . In the following we will only show results from model number 6.

The inverted κ_0 for downhole and surface sensors are mapped in Figure 6. Almost all the κ_0 values shown in Figure 6 are positive, except for some downhole values, which are very close to 0.

Figure 7 shows that the κ_0 values downhole and at the surface are correlated. A large (or small) κ_0 at the surface is linked with a large (or small) κ_0 downhole and there is an average shift of 0.015 s. On the one hand, the shift indicates the influence of shallow layers (between downhole and surface) on κ . On the other hand, the correlation shows that a significant contribution to κ_0 originates deeper than the borehole sensor (since κ still exists downhole). However, there are no apparent regional variations of κ_0 (Figure 6).

The histograms shown in Figure 7 indicate an average κ_0 of 0.033 s at the surface, and of 0.017 s downhole. The standard deviation is slightly higher at the surface than at depth. Those results are in good agreement with the findings of Oth *et al.* (2011) who found an average κ_0 equal to 0.029 s at the surface and 0.015 s downhole with a slightly lower deviation (0.08 s for both) than ours (0.12 and 0.10, respectively).

To test the site-dependent portion of high-frequency attenuation, Figure 8 shows κ_0 at the surface plotted against several site parameters: V_{S30} , f_0 (the fundamental resonant frequency from H/V computed from earthquake data), V_{Smean} (average velocity between the surface and downhole sensors), V_{S5} , V_{S10} , and V_{S20} . Also plotted are borehole κ_0 against $V_{Sdownhole}$ (the shear wave velocity at the borehole depth). From the KIK-net data only, a correlation between κ_0 and V_{S30} is observed, which is greater than the correlations with V_{S5} , V_{S10} , and V_{S20} , suggesting that V_{S30} is not the worst site effect proxy. However, Figure 8 also shows that a correlation between κ_0 and V_{Smean} exists, of the same order as with V_{S30} , which indicates that the origin of κ_0 is not only due to the top 30 meters. When the difference between the surface and downhole κ_0 's is plotted against V_{S30} , the correlation is better, confirming that a part of the κ_0 results from the shallower layers. This is also supported by the small correlation between κ_0 and f_0 which emphasize the importance of the depth of the sedimentary layers as shown by Campbell (2009). The same is true looking at the correlation between κ_0 downhole and $V_{Sdownhole}$, which indicates an even deeper origin of κ_0 .

The source component of κ (κ_{source}) is shown in Figure 9. Clear regional variations can be observed. There is no obvious trend of κ_{source} as a function

of magnitude or focal depth of the earthquake. Such a pattern could be the result of lateral variations of attenuation. Indeed, Pei *et al.* (2009) produce a tomographic image of Japan showing a low-Q region in Central Japan linked with volcanic activity. This region coincides with the negative κ_{source} terms. One other alternative cause could be the effect of focal mechanism (Purvance and Anderson, 2003).

Finally, the κ_0 - V_{S30} couples that we obtained with the Japanese and the NGA data are plotted on top of results from the literature (Silva *et al.*, 1998; Chandler *et al.*, 2006; Douglas *et al.*, 2010; Drouet *et al.*, 2010; Edwards *et al.*, 2011) (Figure 10). In this case the correlation is clearer even if a large scatter persists. The regression of all the data leads to the following relationship:

$$\ln(\kappa_0) = 3.490(\pm 0.505) - 1.062(\pm 0.076) \times \ln(V_{S30}) \quad (6)$$

with a correlation coefficient of 0.39 and a standard error for the estimated $\ln(\kappa_0)$ of 0.55. This relationship is close to the one proposed by Silva *et al.* (1998) based on California data only. It is also consistent with the worldwide relationship proposed by Chandler *et al.* (2006) for V_{S30} s lower than 1500 m/s. For higher V_{S30} s, the difference is increasing very fast since Chandler *et al.* (2006) used a non-linear form. The data obtained in the present study could also support a non-linear form however considering the large observed variability we prefer to keep a simpler model.

5 Hard rock to standard rock amplification factors

In many stable areas like Western Europe, strong ground motion data are lacking and consequently no specific GMPEs exist for these regions. Several GMPEs for stable areas have been defined for ENA where the rock sites are competent ($V_{S30} > 2000$ m/s). Such very high velocity is not consistent with site conditions at many rock sites where records are available or with the rock definition used in recent PSHA studies (e. g. Share FP7 project at the European scale, <http://www.share-eu.org/>). Therefore, some adjustments to account for the different rock for site conditions are needed based on: 1) the difference in V_{S30} and 2) on associated κ_0 values.

We used 2 ENA GMPEs to develop our adjustments: Toro *et al.* (1997) and Campbell (2003). The procedure is based on the host-to-target adjustment method of Campbell (2003). This method requires a host and target regions, in our case the same region but with different rock site conditions. The host region is the one for which a GMPE exists, and which can be described by seismological parameters (stress drop, quality factor, κ_0 ...). The same set of seismological parameters must be available for the target region. Then using a simulation tool (like for instance SMSIM Boore, 2003), one can compute synthetic ground-motions from the seismological parameters for the two regions. Finally, the ratios between these synthetic predictions are used to adjust the original GMPE (see Campbell, 2003 for details); in other words, a new set of adjusted ground-motion data is produced. The last step is the regression of the new data using the same functional form as for the original

model. The host-to-target procedure has been used in Douglas *et al.* (2006) to derive GMPEs for Norway and Spain. These authors developed a Fortran program called CHEEP, which is used in this study.

For the Campbell (2003) GMPE, the host stochastic seismological parameters are given in the original article. In the case of Toro *et al.* (1997), these parameters are not given but Scherbaum *et al.* (2006) used an inversion procedure to determine the seismological parameters that can best reproduce the ground-motion predictions from a number of popular GMPEs, including Toro *et al.* (1997). These equivalent seismological parameters for the two GMPEs are reproduced in Table 3:

For the stochastic simulations, the site amplifications relative to the V_{S30} were estimated using the generic rock site velocity profiles from Boore *et al.* (1997) (see Cotton *et al.*, 2006, for details on the procedure). To define our target region, we modified the V_{S30} and κ_0 from Table 2, keeping all the other parameters constant.

Our aim is to estimate adjustments from very hard rock to standard rock (and vice-versa) that include uncertainties on κ_0 . Our target generic rock site is defined by $V_{S30}=800$ m/s, given a priori, and a range of probable κ_0 between 0.02 and 0.05 s obtained from Figure 10. As a comparison, Atkinson and Boore (2006) who derived a GMPE for stable continental regions (ENA) define the standard rock with: $V_{S30}=760$ m/s and $\kappa_0=0.01$ to 0.03 s. These κ_0 values seem however low compared to our results shown in Figure 10. On the other hand, very hard rock sites have different definitions depending on the authors:

- Atkinson and Boore (2006): $V_{S30}=2000$ m/s and $\kappa_0=0.002$ to 0.008 s

(uniform distribution)

- Toro *et al.* (1997): $V_{S30}=2800$ m/s and $\kappa_0=0.002, 0.006, \text{ or } 0.012$ s (same probability for the 3 values)
- Campbell (2003): $V_{S30}=2800$ m/s and $\kappa_0=0.002, 0.006, \text{ or } 0.012$ s (the middle value being more probable)

Our procedure requires three steps, which are summarized in Figure 11: 1) adjustment to a generic hard rock site (all combinations of $V_{S30}=2000, 2600, 2800$ m/s and $\kappa_0=0.002, 0.005, 0.01$ s); 2) adjustment to a generic rock ($V_{S30}=800$ m/s and $\kappa_0=0.02, 0.03, \text{ and } 0.05$ s); and 3) estimation of ratios between generic rock and generic hard rock.

Both the adjusted and original models, for a specific magnitude-distance scenario ($M=6, R=20$ km), are shown in Figure 12 for different hard-rock and rock conditions. One can first check that the adjustments (correction of original spectral amplification by the ratios of target and host Fourier amplitudes plus new regression) with the original very hard rock site definition leads to models equivalent to the original GMPEs. However, we observed that the adjustment of the Toro *et al.* (1997) GMPE performs poorly for distances greater than 100 km, which is not the case for the Campbell (2003) GMPE. This is probably due to the set of parameters used. Indeed the equivalent stochastic parameters determined by Scherbaum *et al.* (2006) are valid up to distances of 100 to 200 km. In the following we will not use the adjusted Toro *et al.* (1997) GMPEs for distances greater than 100 km. For the rock adjustment, lowering the V_{S30} value increases the spectral amplitudes at all periods, but this effect is counter-balanced by a drastic decrease of the

amplitudes due to higher κ_0 values, especially for periods lower than 0.5 s.

We then compute the ratios between the original and adjusted models for a number distances and magnitudes (R=1, 2, 3, 5, 10, 20, 30, 50, 100, 200, 300, 500 km; M=5, 6, 7). Distances greater than 100 km are not used in the case of the Toro *et al.* (1997) GMPE as explained above. The results are shown in Figure 13. The average ratios can be seen as the ratios between the original GMPE (Toro *et al.* (1997) or Campbell (2003)) and generic hard rock or rock models.

As a comparison, Atkinson and Boore (2006) give two sets of coefficients for very hard and hard rock sites, and we computed the same ratios between very hard rock and rock predictions. Those are also plotted in Figure 14. The low κ for rock sites chosen by Atkinson and Boore (2006) are leading to low amplitude ratios compared to the ratios computed using the Toro *et al.* (1997) and the Campbell (2003) GMPEs.

Our final aim is to take into account the uncertainty associated with the very hard rock definition for both V_{S30} and κ_0 , and with the κ_0 which has to be assigned to a rock site defined by $V_{S30}=800$ m/s, to compute ratios for converting motions from very hard rock sites to motion for rock sites. This is achieved by computing the ratios between the average ratios of Figure 13 (shown as note $ratio_{Very\ hard\ rock}$ and $ratio_{Rock}$, respectively):

$$\begin{aligned}
 Final\ ratio &= \frac{ratio_{Very\ hard\ rock}}{ratio_{Rock}} \\
 \sigma_{Final\ ratio} &= \sqrt{\left(\frac{\sigma_{Very\ hard\ rock}}{ratio_{Rock}}\right)^2 + \left(\frac{\sigma_{Rock} \times ratio_{Very\ hard\ rock}}{ratio_{Rock}^2}\right)^2} \quad (7)
 \end{aligned}$$

We end up with the ratios between a generic rock site (with $V_{S30}=800$

m/s and κ_0 ranging between 0.02 and 0.05 s) and a generic very hard rock site (with V_{S30} ranging between 2000 and 2800 m/s and κ_0 ranging between 0.002 and 0.01 s). These final ratios are obtained for both Toro *et al.* (1997) and Campbell (2003) models and are shown in Figure 15, together with the average ratios from Atkinson and Boore (2006). Again the rock site κ_0 used by Atkinson and Boore (2006) is rather low compared to the results of Figure 10, which explains the slightly higher amplitude ratios in this case.

It appears from Figure 15 that the results using the Toro *et al.* (1997) GMPE and Campbell (2003) GMPE are consistent and similar. The final ratios have close mean and standard deviation at each period, while the ratios estimated from Atkinson and Boore (2006) present higher values and lower standard deviations due to the low rock site κ_0 these authors used. Finally, we suggest to keep and use the ratios computed with the Campbell (2003) since there are no distance limitations as in the case of Toro *et al.* (1997) (as explained previously). The final ratios using Campbell (2003) GMPE have been interpolated to cover a large range of periods and can be used as a proxy to perform the very-hard to hard rock adjustment (see Fig. 15 and Table S3 available as an electronic supplement to this paper). Further analysis using other GMPEs for stable continental regions could help to check the stability of the ratio.

6 Discussion and conclusion

In this study, a large amount of data from Japan (KIK-net) and from the NGA database are used to determine the high-frequency decay of the Fourier

spectra. The data are of very good quality, with mostly digital sensors, and are characterized by measured V_{S30} 's. After a visual check of all the data and a manual picking of P- and S-waves, we determined the high-frequency decay parameter κ by regression of the Fourier amplitude against frequency in a log-lin space. One has to note that the site effect may have biased the results obtained with surface sensors since high-frequency site effects have been observed in Japan (Oth *et al.*, 2011).

In order to correct for this effect and determine site-specific κ -values: κ_0 , we used two options depending on the data set. The first one consists for each station to simply extrapolate the data to $r=0$, following the slope determined regionally. This was applied to the NGA data. The second options, which was used with the KIK-net data thanks to the large amount of data, is to invert for the κ_0 -values, the regional slope and a source term for κ simultaneously.

For Japan we choose a nation-wide attenuation term. Lateral variations of the attenuation properties have been obtained from tomography study linked with volcanic activity or density of faults (Pei *et al.*, 2009). However, variations of the quality factor are small (Oth *et al.*, 2011) and have consequently a small impact on the Fourier amplitude spectra. The slopes of the κ versus distance plot that were determined in Japan show that attenuation for shallow events is higher than that obtained for deep events. This was expected since the waves are sampling less attenuating material (i.e. part of the mantle) for the deeper earthquakes. Finally, the slopes obtained on surface for Japan, California and Taiwan are rather different, highlighting different attenuation properties in the three regions.

We also determined a source component of κ , which is not negligible and shows regional variations. The amplitude of the source component is slightly less than the amplitude of the site component. No correlation with magnitude or depth could be observed. These regional variations in the source component could result from regional variations of attenuation which are not properly taken into account. Although, regional variations of Q have a small impact on the Fourier amplitude spectra, they might however influence the source components of κ which have a low amplitude. For example, the high attenuation area observed by Pei *et al.* (2009) coincides with our low κ_{source} terms zone. Moreover, Castro *et al.* (2000) found that small-scale variations of Q can significantly affect κ values. Another possible reason could be the focal mechanism of the event or the maturity of the fault, as proposed by Purvance and Anderson (2003). Some work is still needed to clearly discriminate source and propagation effect on κ .

The arrangement of the KIK-net stations with two sensors, one on the surface and one at depth in a borehole, allowed us to check the correlation between κ_0 (at the surface and at depth) and various site parameters: V_{S30} , V_{S20} , V_{S10} , V_{S5} , V_{Smean} , $V_{Sdownhole}$, f_0 . The results show that the correlation between κ_0 and superficial site properties (V_{S30}) is not better than with deeper properties (V_{Smean}). However, the even smaller correlations with V_{S20} , V_{S10} , or V_{S5} indicates that V_{S30} is the best site proxy among the 4. Since the pioneering study of Hough *et al.* (1988), the link between the high-frequency decay and site properties is clearly established. It has been often assumed that κ_0 is linked with the attenuation of the uppermost layers. However, Campbell (2009) showed that the depth of the sedimentary column was also

important, supporting the idea of a deeper origin than previously envisaged. This study supports Campbell (2009) results but we also suggest an even deeper origin of κ_0 . The analysis performed with the downhole sensors show a correlation between the κ_0 measured at depth and the velocity at depth. This suggests that the structure below the station down to some kilometers could have an influence on κ .

The correlation between κ_0 and V_{S30} becomes more convincing when data from other studies are superimposed (Figure 10). However, a large variability exists which could be explained by source effects and the deep origin of κ mentioned above. Those correlations are important in the context of GMPE rock to very hard rock (and vice-versa) adjustments. Based on the κ_0 - V_{S30} correlation determined, we could define domains relative to rock and very hard rock sites. Then using the Campbell (2003) host-to-target adjustment method, we adjusted Toro *et al.* (1997) and Campbell (2003) GMPEs from very hard rock sites to rock sites. The comparison of the ratios between the two models fit nicely. These ratios have lower amplitude than those obtained from Atkinson and Boore (2006), who derived a GMPE for both rock and very hard rock sites. This is explained by the fact that Atkinson and Boore (2006) gave a narrow band of probable κ_0 's in their rock site definition. The ratios determined in the present study can be used to convert ground-motion prediction for very hard rock sites ($V_{S30}>2000$ m/s) to ground-motion prediction for rock site ($V_{S30}=800$ m/s).

7 Data and resources

Accelerograms and geotechnical data from the KIK-net network are available at <http://www.kik.bosai.go.jp> (last access June 2011). Accelerograms and associated metadata from the NGA project at <http://peer.berkeley.edu/nga/> (last access June 2011).

8 Acknowledgments

The authors would like to warmly thank John Douglas who shared his code CHEEP which performs host-to-target adjustment, Aldo Zollo and his team at RISSC-LAB (Napoli) for making the selection of KIK-net data available to us, the PEER-NGA project participants for building an extremely rich accelerometric database. This work wouldn't have been possible without the huge amount of work from KIK-net network staff (NIED) that provide the seismological community with amazing data. The authors would also like to thank the Associated Editor, Ivan G. Wong, and the two anonymous reviewers for their comments which helped to improve the manuscript. This work has been supported by the European Commission through the FP7-ENVIRONMENT-226967 project entitled 'Seismic Hazard Harmonization in Europe' (SHARE) and the FP7-PEOPLE-248182 project entitled 'Ground-motion modelling for seismic hazard assessment in regions with moderate to low seismic activity'. Fabrice Cotton's work is also supported by Institut Universitaire de France. This study originates from the dissertation research project of Chris Van Houtte to obtain the master's degree in

Earthquake Engineering and Engineering Seismology (MEEES Consortium: www.meees.org).

References

- Aki, K. (1967). Scaling law of seismic spectrum. *J. Geophys. Res.*, **72**, 1217–1231.
- Anderson, J. G. and S. E. Hough (1984). A model for the shape of the fourier amplitude spectrum of acceleration at high frequencies. *Bull. Seism. Soc. Am.*, **74**, 1969–1993.
- Atkinson, G. M. and D. M. Boore (2006). Earthquake ground-motion prediction equations for Eastern North America. *Bull. Seism. Soc. Am.*, **96**, 2181–2205.
- Bommer, J. J., J. Douglas, F. Scherbaum, F. Cotton, H. Bungum, and D. Fäh (2010). On the selection of ground-motion prediction equations for seismic hazard analysis. *Seismol. Res. Lett.*, **81**, 783–793.
- Boore, D. (1983). Stochastic simulation of high-frequency ground motions based on seismological models of the radiated spectra. *Bull. Seism. Soc. Am.*, **73**, 1865–1894.
- Boore, D. M. (2003). Simulation of ground motion using the stochastic method. *Pure Appl. Geophys.*, **160**, 635–676.
- Boore, D. M., W. B. Joyner, and T. E. Fumal (1997). Equations for estimating horizontal response spectra and peak acceleration from western North

- American earthquakes: a summary of recent works. *Seismol. Res. Lett.*, **68**, 128–153.
- Brune, J. N. (1970). Tectonic stress and the spectra of seismic shear waves from earthquakes. *J. Geophys. Res.*, **75**, 4997–5009.
- Cadet, H., P.-Y. Bard, and A. Rodriguez-Marek (2010). Defining a standard rock site: propositions based on the KIK-net database. *Bull. Seism. Soc. Am.*, **100**, 172–195.
- Campbell, K. W. (2003). Prediction of strong ground motion using the hybrid empirical method and its use in the development of ground-motion (attenuation) relations in eastern North America. *Bull. Seism. Soc. Am.*, **93**, 1012–1033.
- Campbell, K. W. (2009). Estimates of shear-wave Q and κ_0 for unconsolidated and semiconsolidated sediments in Eastern North America. *Bull. Seism. Soc. Am.*, **99**, 2365–2392.
- Castellaro, S., F. Mulargia, and P. L. Rossi (2008). v_{S30} : Proxy for seismic amplification? *Seismol. Res. Lett.*, **79**, 540–543.
- Castro, R. R., L. Trojani, G. Monachesi, M. Mucciarelli, and M. Cattaneo (2000). The spectral decay parameter κ in the region of Umbria-Marche, Italy. *J. Geophys. Res.*, **105**, 23,811–23,823.
- Chandler, A. M., N. T. K. Lam, and H. H. Tsang (2006). Near-surface attenuation modelling based on rock shear-wave velocity profile. *Soil Dyn. Earthq. Eng.*, **26**, 1004–1014.

- Chiou, B. S.-J., R. Darragh, N. Gregor, and W. Silva (2008). NGA Project Strong-Motion Database. *Earthquake Spectra*, **24**, 23–44.
- Cotton, F., F. Scherbaum, J. J. Bommer, and H. Bungum (2006). Criteria for selecting and adjusting ground-motion models for specific target regions: Application to Central Europe and rock sites. *J. Seismology*, **10**, doi:10.1007/s10,950–005–9006–7.
- Douglas, J., H. Bungum, and F. Scherbaum (2006). Ground-motion prediction equations for Southern Spain and Southern Norway obtained using the composite hybrid model perspective. *J. Earthq. Eng.*, **10**, 33–72.
- Douglas, J., P. Gehl, L. F. Bonilla, and C. Gelis (2010). A kappa model for mainland France. *Pure Appl. Geophys.*, **167**, 1303–1315.
- Drouet, S., F. Cotton, and P. Guéguen (2010). v_{S30} , κ , regional attenuation and M_w from small magnitude events accelerograms. *Geophys. J. Int.*, **182**, 880–898.
- Edwards, B., D. Faeh, and D. Giardini (2011). Attenuation of seismic shear-wave energy in Switzerland. *Geophys. J. Int.*, **185**, 967–984.
- Fujiwara, H., S. Aoi, T. Kunugi, and S. Adachi (2004). Strong-motion Observation Networks of NIED: K-NET and KiK-net. Technical report, Consortium of Organizations for Strong-Motion Observation Systems (COSMOS). [Http://www.cosmos-eq.org/events/wkshop_records_processing/presentations/Fujiwara.pdf](http://www.cosmos-eq.org/events/wkshop_records_processing/presentations/Fujiwara.pdf).
- Hanks, T. C. (1982). fmax. *Bull. Seism. Soc. Am.*, **72**, 1867–1879.

- Hough, S. E., J. G. Anderson, J. Brune, F. Vernon, J. Berger, and J. Fletcher (1988). Attenuation near Anza, California. *Bull. Seism. Soc. Am.*, **78**, 672–691.
- McGuire, R. K. (1978). A simple model for estimating Fourier amplitude spectra of horizontal ground acceleration. *Bull. Seism. Soc. Am.*, **68**, 803–822.
- Oth, A., D. Bindi, S. Parolai, and D. D. Giacomo (2011). Spectral analysis of K-NET and KIK-net data in Japan, Part II: on attenuation characteristics, source spectra, and site response of borehole and surface stations. *Bull. Seism. Soc. Am.*, **101**, 667–687.
- Papageorgiou, A. S. and K. Aki (1983). A specific barrier model for the quantitative description of inhomogeneous faulting and the prediction of strong ground motion. *Bull. Seism. Soc. Am.*, **73**, 693–722.
- Parolai, S. and D. Bindi (2004). Influence of soil-layer properties on k evaluation. *Bull. Seism. Soc. Am.*, **94**, 349–356.
- Pei, S., Z. Cui, Y. Sun, M. N. Toksöz, C. A. Rowe, X. Gao, J. Zhao, H. Liu, J. He, and F. D. Morgan (2009). Structure of the upper crust in Japan from S-wave attenuation tomography. *Bull. Seism. Soc. Am.*, **99**, 428–434.
- Purvance, M. D. and J. G. Anderson (2003). A comprehensive study of the observed spectral decay in strong-ground accelerations recorded in Guerrero, Mexico. *Bull. Seism. Soc. Am.*, **93**, 600–611.
- Scherbaum, F., F. Cotton, and H. Staedtke (2006). The estimation of

minimum-misfit stochastic models from empirical ground-motion prediction equations. *Bull. Seism. Soc. Am.*, **96**, 427–445.

Silva, W. and R. B. Darragh (1995). Engineering characterization of strong ground motion recorded at rock sites. Technical report, Electric Power Research Institute, El Cerrito, California. EPRI Report TR-102262.

Silva, W., R. B. Darragh, N. Gregor, G. Martin, N. Abrahamson, and C. Kircher (1998). Reassessment of site coefficients and near-fault factors for building code provisions. *Technical Report Program Element II: 98-HQ-GR-1010, Pacific Engineering and Analysis, El Cerrito, USA.*

Toro, G. R., N. A. Abrahamson, and J. F. Schneider (1997). Model of strong ground motions for earthquakes in central eastern North America: best estimates and uncertainties. *Seismol. Res. Lett.*, **68**, 41–57.

Tsai, C.-C. P. and K.-C. Chen (2000). A model for the high-cut process of strong-motion accelerations in terms of distance, magnitude, and site condition: an example from the SMART 1 Array, Lotung, Taiwan. *Bull. Seism. Soc. Am.*, **90**, 1535–1542.

List of Tables

1	Number of events, stations and records for the Japanese and NGA data sets.	30
2	Tests on different parametrizations of κ for the analysis of the KIK-net data	30
3	Host stochastic parameters.	30

Table 1: Number of events, stations and records for the Japanese and NGA data sets.

Region		Number of events	Number of stations	Number of records
Japan	Total	404	161	6318
	Events with depth ≤ 25 km	267	160	4554
	Events with depth > 25 km	137	113	1718
NGA	USA, California	21	44	91
	Taiwan	6	27	99

Table 2: Tests on different parametrizations of κ for the analysis of the KIK-net data

Model	$\sigma_{residuals}$	F-test	F-test probability
1) κ_0	0.0083		
2) κ_{source}	0.0134	(1/2) 2.67	(1/2) 0.0
3) $\kappa_0 + \kappa_{source}$	0.0074	(1/3) 1.25	(1/3) 0.4e-13
4) $\kappa_0 +$ distance term	0.0076	(1/4) 1.20	(1/4) 0.6e-9
5) $\kappa_{source} +$ distance term	0.0132	(4/5) 3.10	(4/5) 0.0
6) $\kappa_0 + \kappa_{source} +$ distance term	0.0069	(4/6) 1.22	(4/6) 0.5e-10

Table 3: Host stochastic parameters.

GMPE	Stress drop (bar)	κ_0 (sec)	Geometrical spreading exponent	Quality factor	V_{S30} (m/s)	Duration parameter
Toro <i>et al.</i> (1997) (1)	198	0.01	-0.826 if $1 \geq R < 29.3$ -0.998 if $29.3 \geq R < 97.3$ -0.5 if $R \geq 97.3$	$225 \times f^{0.613}$	3000	0.067
Campbell (2003) (2)	150	0.006	-1.000 if $1 \geq R < 70.0$ 0.000 if $70.0 \geq R < 130.0$ -0.5 if $R \geq 130.0$	$680 \times f^{0.36}$	2800	0.04

(1) equivalent stochastic parameters (Scherbaum *et al.*, 2006)

(2) stochastic parameters for ENA (Campbell, 2003)

List of Figures

1	Top: Map of the stations and events from the KIK-net data analyzed in this study. Bottom: magnitude-distance scatter of the recordings and depth distribution of the events.	34
2	Top: Maps of the stations and events from the NGA data analyzed in this study: Bottom: magnitude-distance scatter of the recordings.	35
3	Example spectra for one earthquake in each region (Japan, Taiwan and California). Data are plotted in dark grey, noise (when available) in light grey, and the linear fit in black. The estimated κ from the regression slope are also indicated for each component.	36
4	Top: Example of site effects estimated at station SITH05: H/V, SSR using the borehole sensor as reference, theoretical transfer function computed from the velocity profile. Bottom: Example of site correction applied to one specific record. . . .	37
5	Regional distance-dependence of κ for: (left) Japan downhole κ 's (top) and surface κ 's (bottom) (dark grey circles: crustal events data; light grey circles: subduction events data); (right) NGA data from California (top) and from Taiwan (bottom). . .	38
6	Site component of κ (κ_0) for downhole sensors (top) and surface sensors (bottom).	39

7	Left: Comparison of the downhole and surface κ_0 's. The solid line shows the 1:1 relationship and the dotted line shows the linear regression of the data. Middle and right: Histograms of κ_0 (middle: downhole; left: surface). The best fit Gaussian curve is also indicated (black curves) with the corresponding parameters (median and standard deviation) above the frames.	40
8	Top: surface κ_0 against V_{S30} (left), f_0 (middle) and V_{Smean} (right). Middle: surface κ_0 against V_{S5} (left), V_{S10} (middle) and V_{S20} (right). Bottom: downhole κ_0 against $V_{Sdownhole}$ (left), and surface κ_0 minus downhole κ_0 against V_{S30} (middle) and V_{Smean} (right).	41
9	Top: Map of the source component of κ . Bottom: Source component of κ against magnitude and depth of the event.	42
10	κ_0 - V_{S30} data from various papers (see legend) and from the present study (left). The same data are plotted together with the correlations from Silva <i>et al.</i> (1998), Chandler <i>et al.</i> (2006) and from the present study (right).	43
11	Flowchart of the estimation of rock to hard rock adjustments.	43
12	Ground-motion predictions for a M=6, R=20 km scenario using Toro <i>et al.</i> (1997) GMPE (left) and Campbell (2003) GMPE (right). Adjusted models to "hard rock-site" conditions are shown in top frames and to "rock-site" conditions in bottom frames.	44

13	Ratios between the original model (left: Toro <i>et al.</i> (1997); right: Campbell (2003)) and the adjusted ones to hard rock conditions (top) and to rock conditions (bottom). The ratios are computed for several magnitudes and distances (see text). Average ratios and error bars are plotted in red.	45
14	Ratios between hard rock and rock ground motion predictions using Atkinson and Boore (2006) GMPE. Average ratios and error bars are plotted in red.	46
15	Average rock to very hard rock ratios estimated using: Atkinson and Boore (2006) GMPE (green), Toro <i>et al.</i> (1997) GMPE (blue), and Campbell (2003) GMPE (red). The black curve is the interpolation of the ratios computed using Campbell (2003).	46

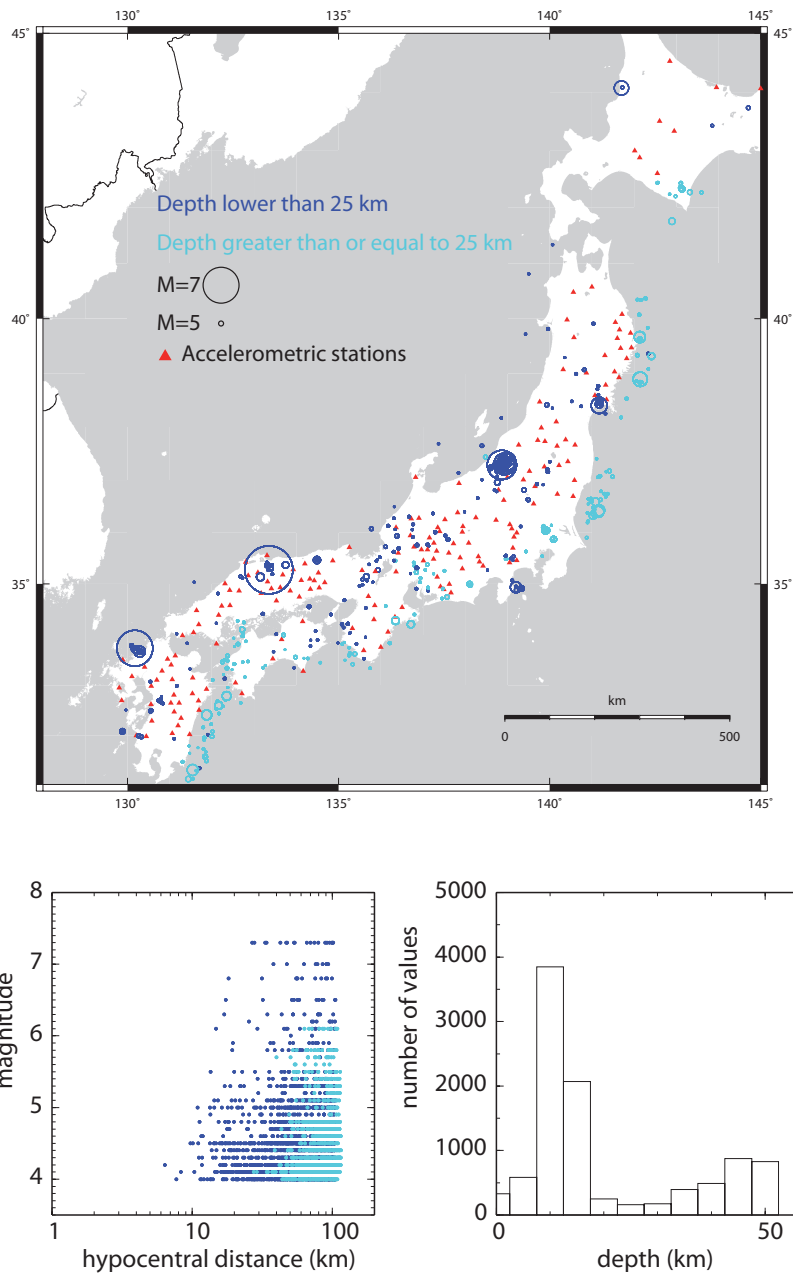


Figure 1: Top: Map of the stations and events from the KIK-net data analyzed in this study. Bottom: magnitude-distance scatter of the recordings and depth distribution of the events.

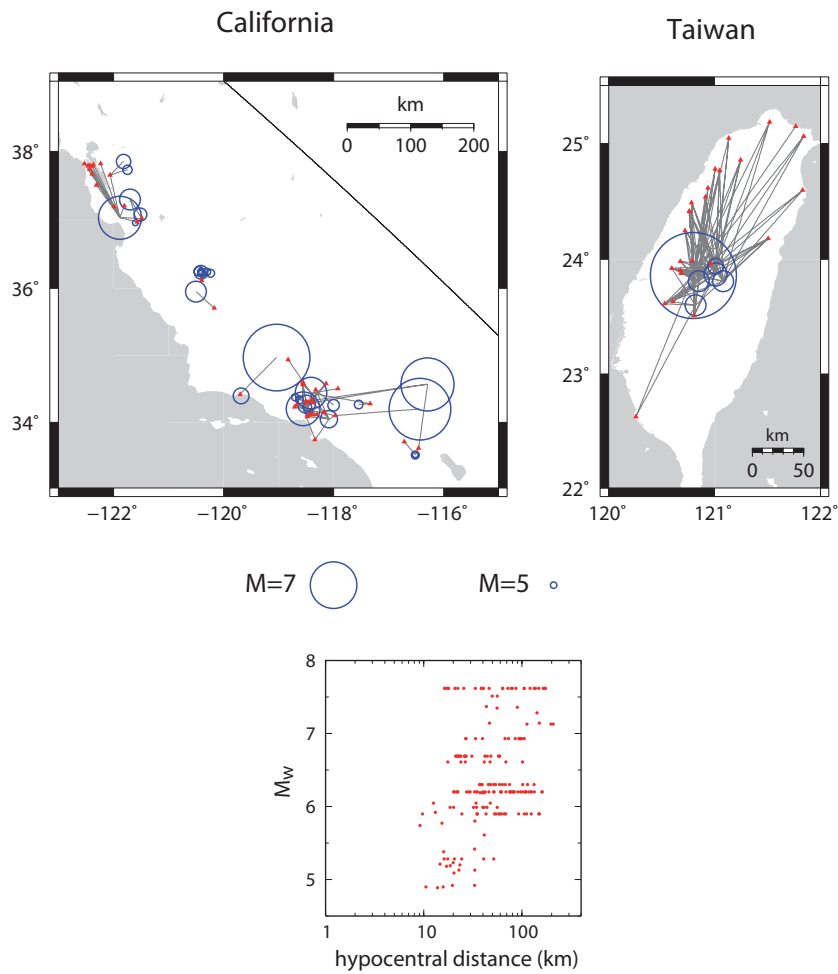


Figure 2: Top: Maps of the stations and events from the NGA data analyzed in this study: Bottom: magnitude-distance scatter of the recordings.

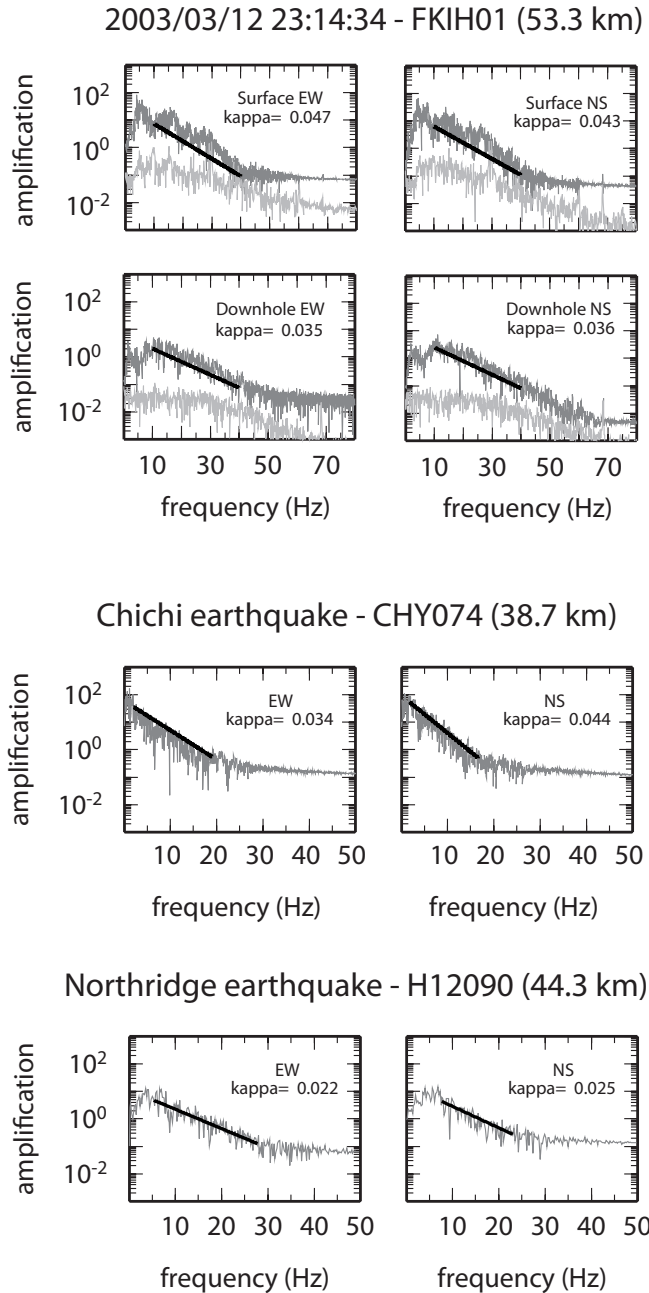
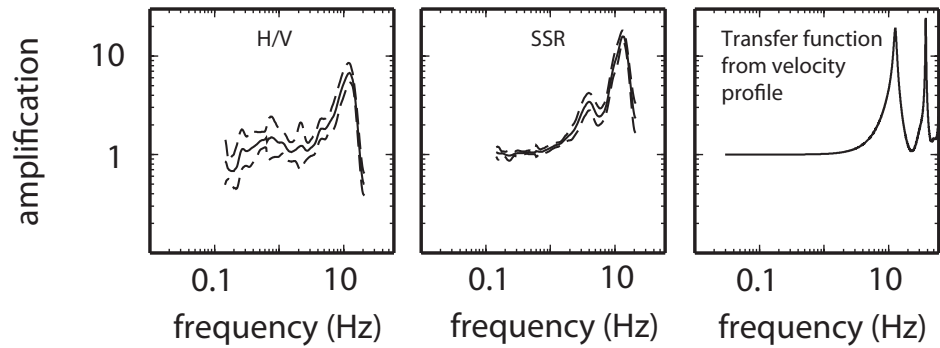


Figure 3: Example spectra for one earthquake in each region (Japan, Taiwan and California). Data are plotted in dark grey, noise (when available) in light grey, and the linear fit in black. The estimated κ from the regression slope are also indicated for each component.



2003/04/08 04:17 - SITH05 (77.8 km - surface NS)

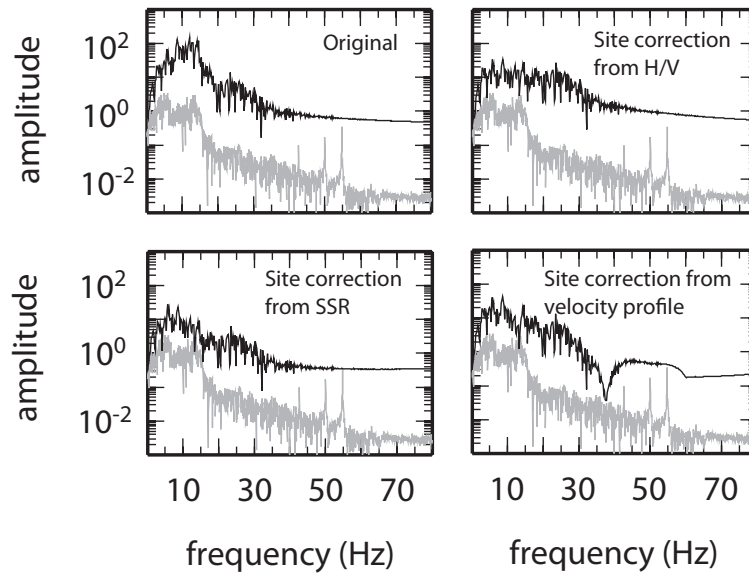


Figure 4: Top: Example of site effects estimated at station SITH05: H/V, SSR using the borehole sensor as reference, theoretical transfer function computed from the velocity profile. Bottom: Example of site correction applied to one specific record.

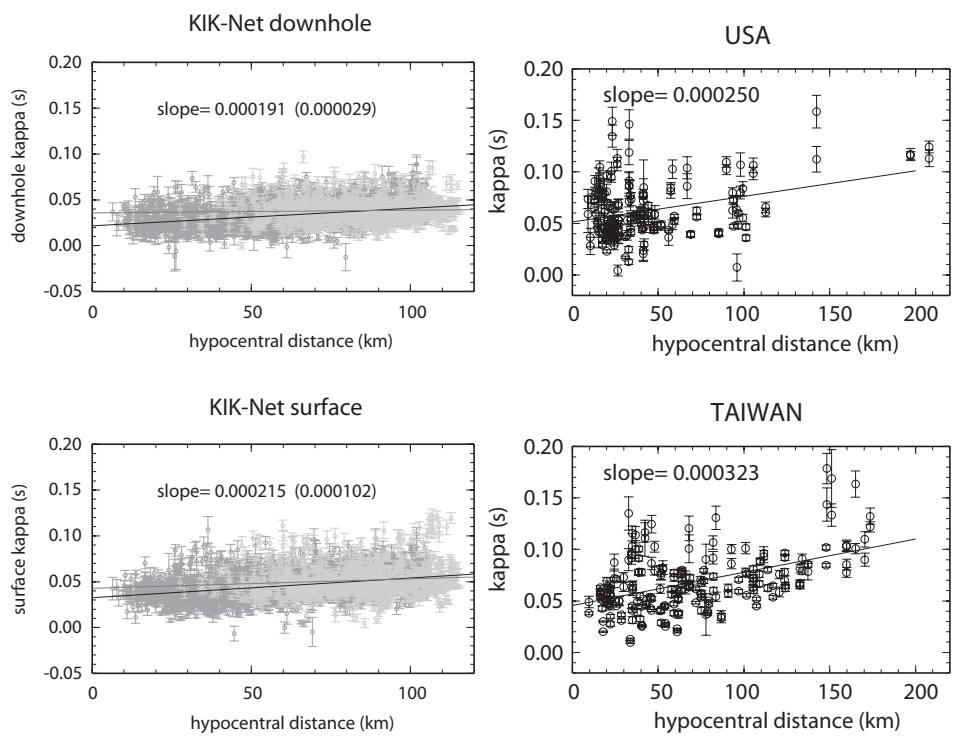


Figure 5: Regional distance-dependence of κ for: (left) Japan downhole κ 's (top) and surface κ 's (bottom) (dark grey circles: crustal events data; light grey circles: subduction events data); (right) NGA data from California (top) and from Taiwan (bottom).

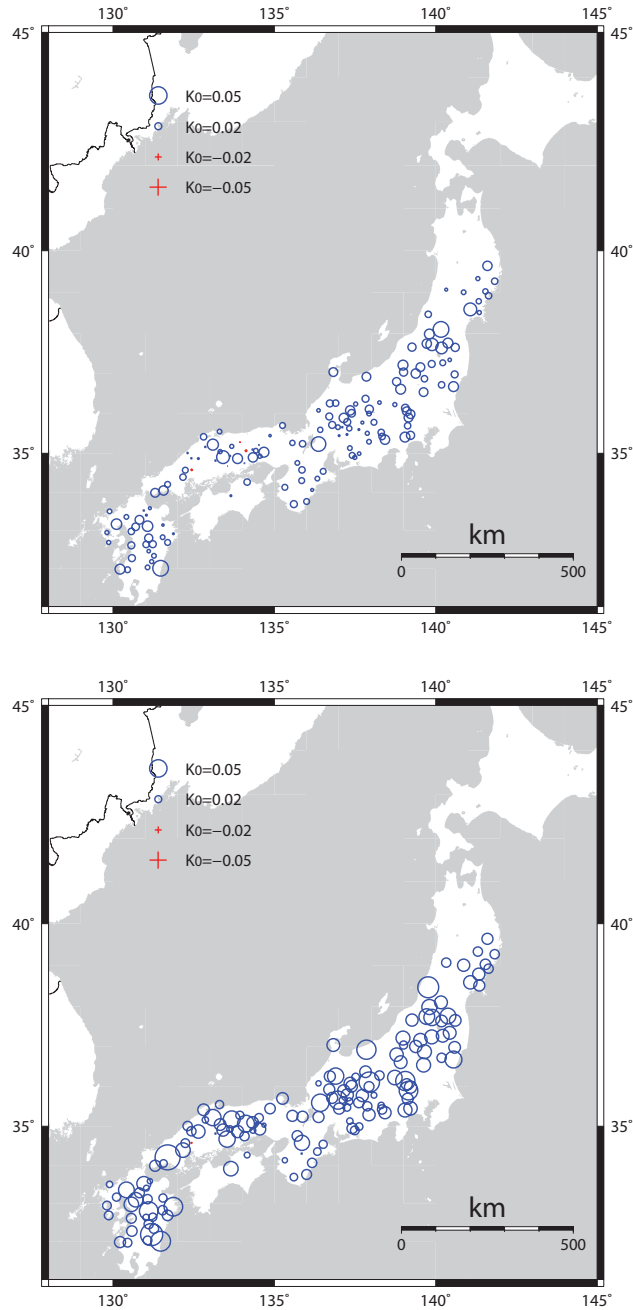


Figure 6: Site component of κ (κ_0) for downhole sensors (top) and surface sensors (bottom).

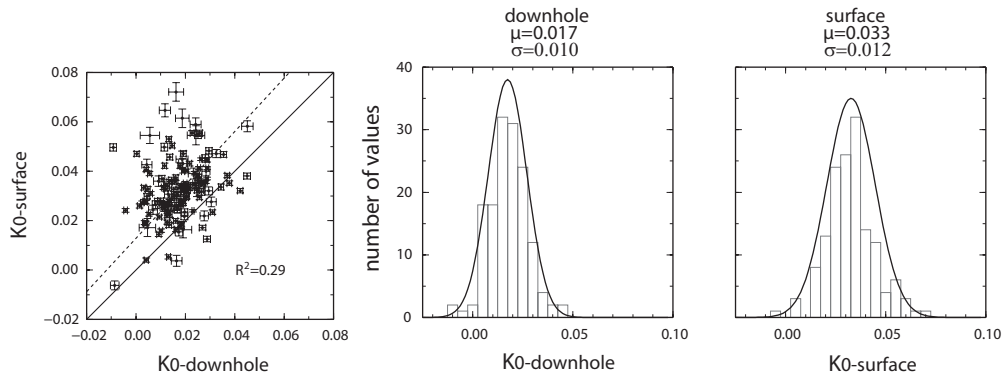


Figure 7: Left: Comparison of the downhole and surface κ_0 's. The solid line shows the 1:1 relationship and the dotted line shows the linear regression of the data. Middle and right: Histograms of κ_0 (middle: downhole; left: surface). The best fit Gaussian curve is also indicated (black curves) with the corresponding parameters (median and standard deviation) above the frames.

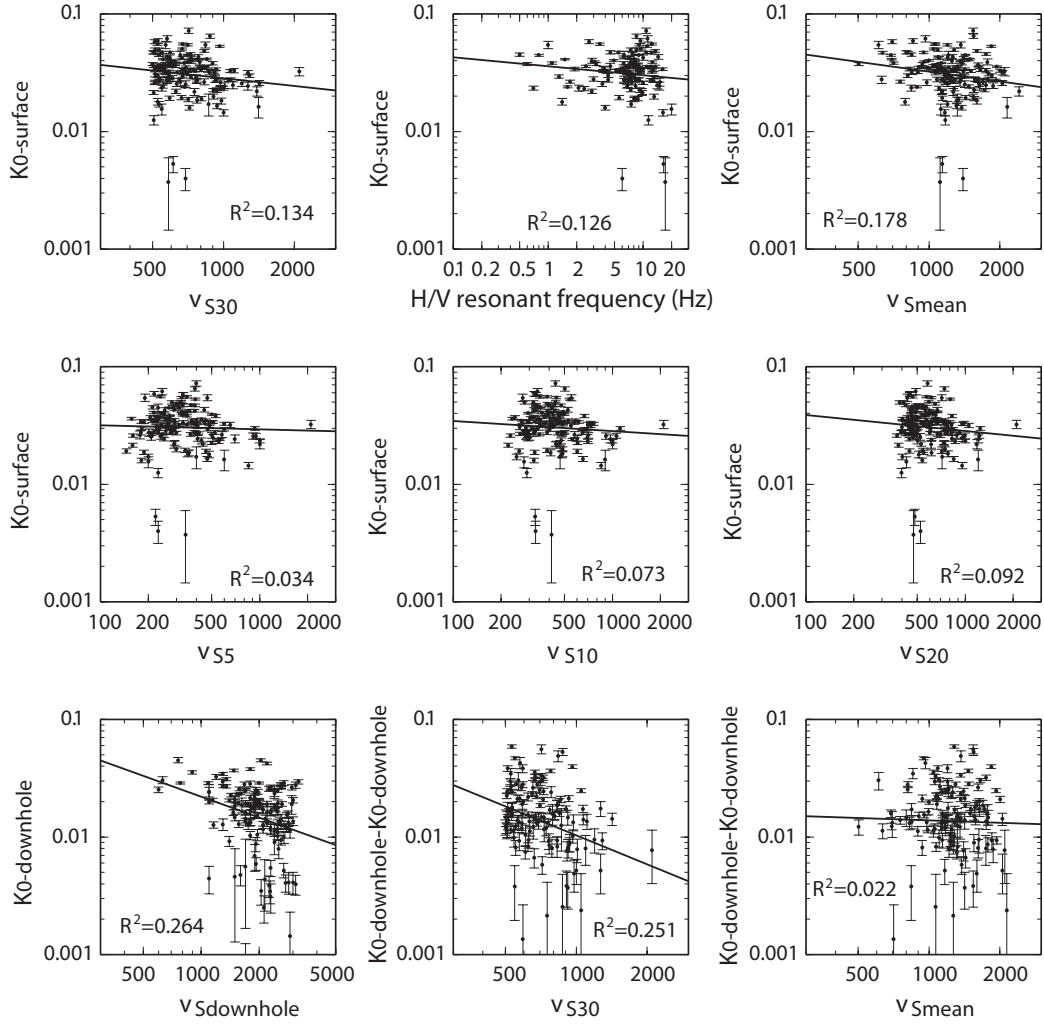


Figure 8: Top: surface κ_0 against V_{S30} (left), f_0 (middle) and V_{Smean} (right). Middle: surface κ_0 against V_{S5} (left), V_{S10} (middle) and V_{S20} (right). Bottom: downhole κ_0 against $V_{Sdownhole}$ (left), and surface κ_0 minus downhole κ_0 against V_{S30} (middle) and V_{Smean} (right).

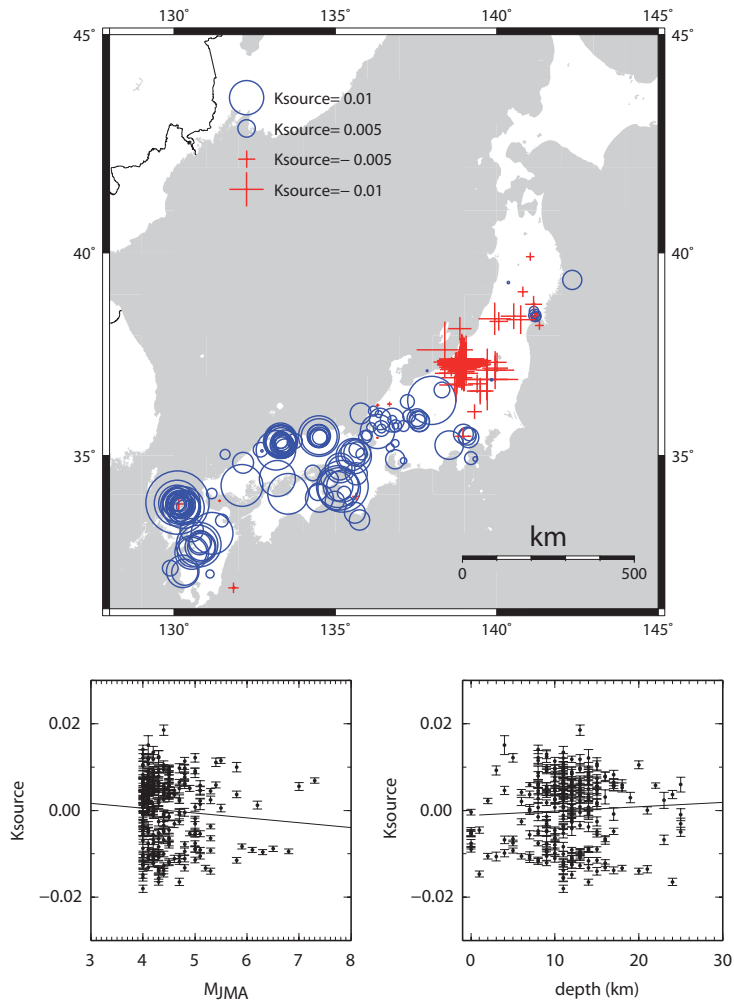


Figure 9: Top: Map of the source component of κ . Bottom: Source component of κ against magnitude and depth of the event.

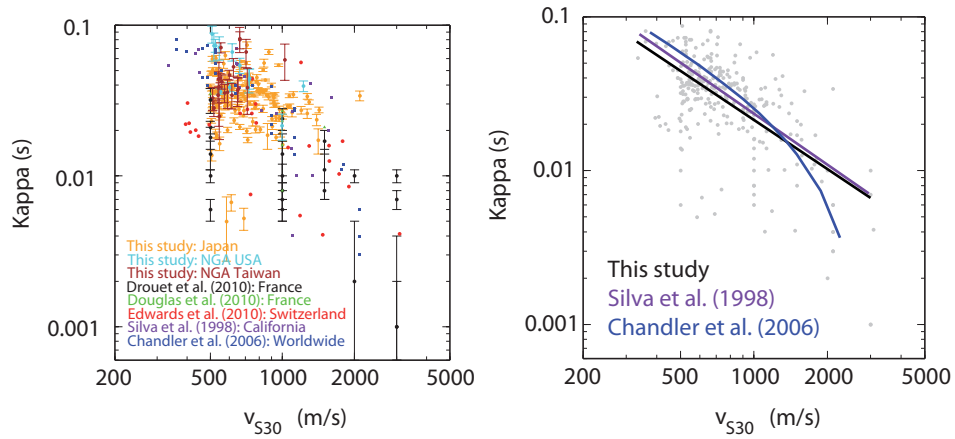


Figure 10: κ_0 - V_{S30} data from various papers (see legend) and from the present study (left). The same data are plotted together with the correlations from Silva *et al.* (1998), Chandler *et al.* (2006) and from the present study (right).

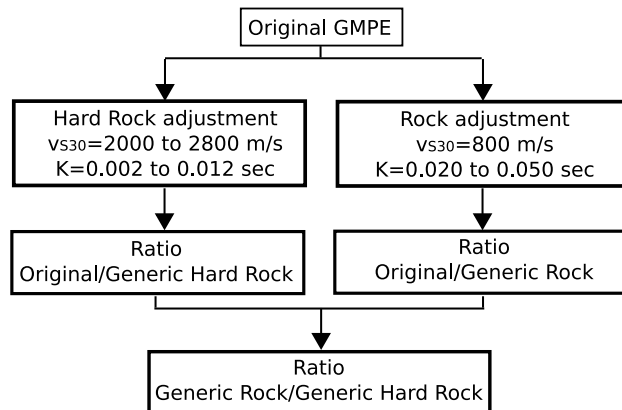


Figure 11: Flowchart of the estimation of rock to hard rock adjustments.

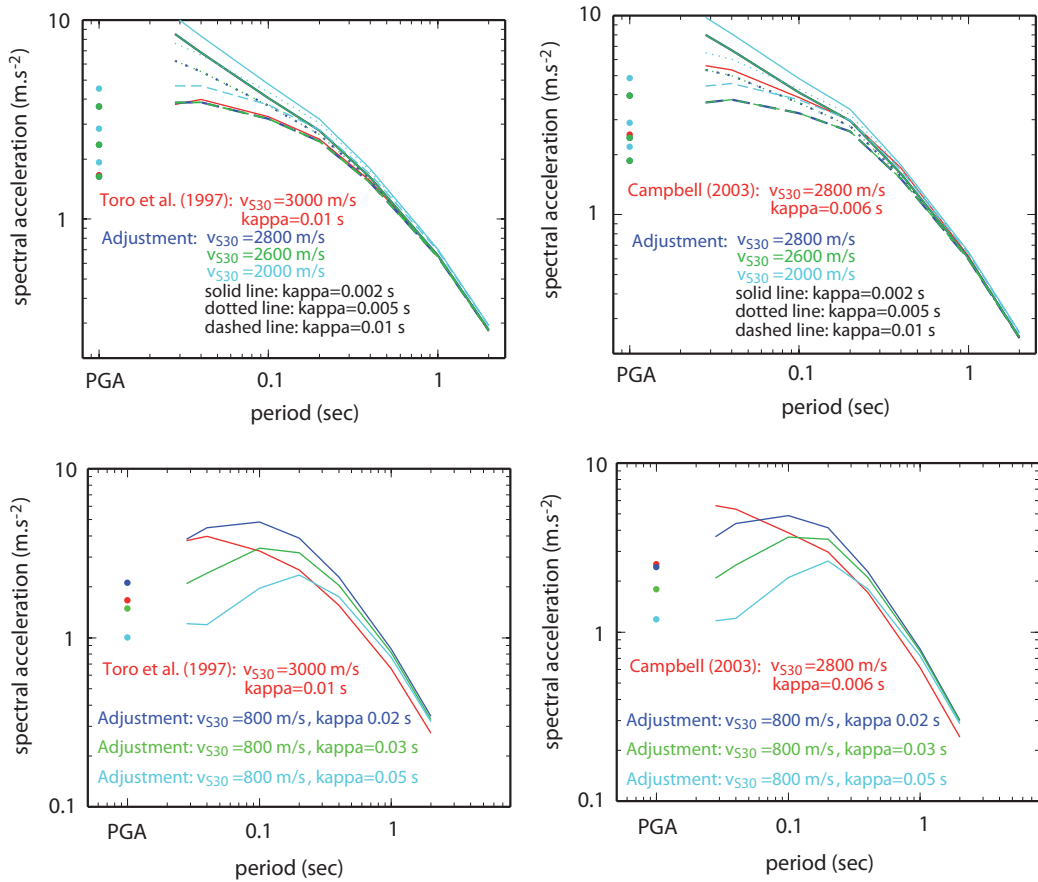


Figure 12: Ground-motion predictions for a M=6, R=20 km scenario using Toro *et al.* (1997) GMPE (left) and Campbell (2003) GMPE (right). Adjusted models to "hard rock-site" conditions are shown in top frames and to "rock-site" conditions in bottom frames.

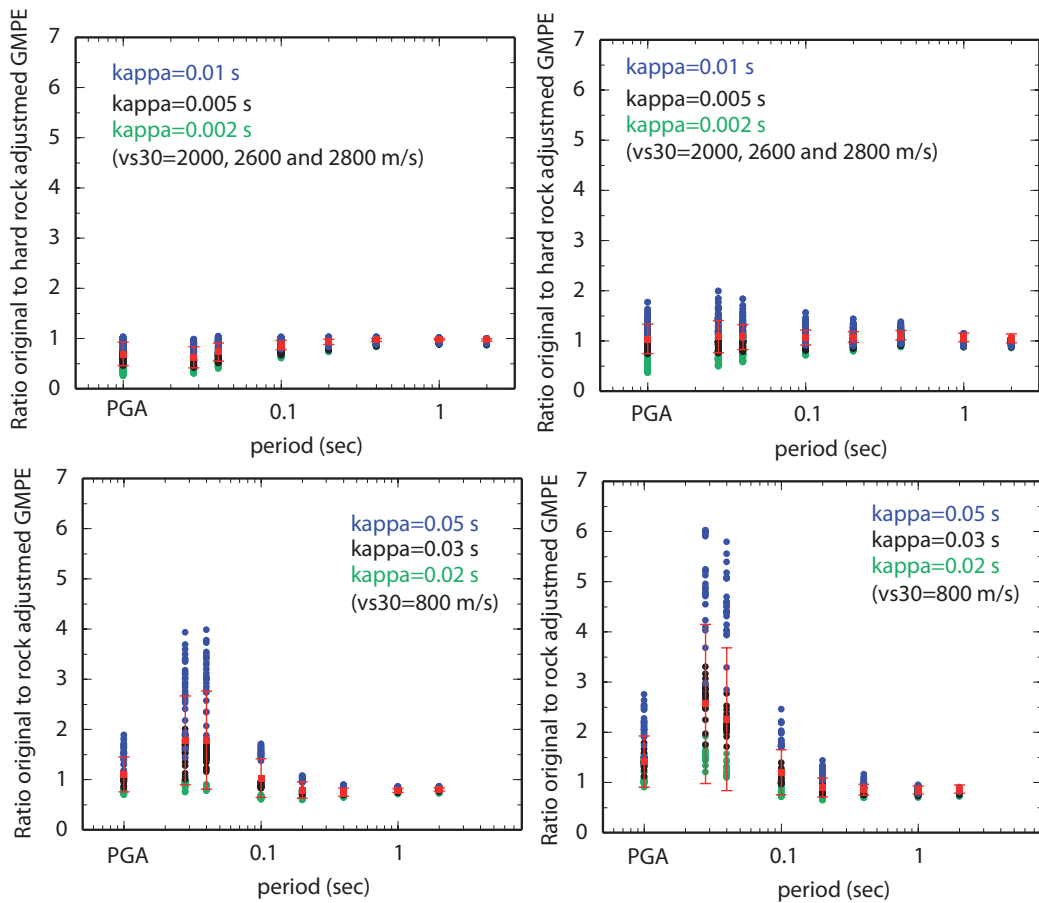


Figure 13: Ratios between the original model (left: Toro *et al.* (1997); right: Campbell (2003)) and the adjusted ones to hard rock conditions (top) and to rock conditions (bottom). The ratios are computed for several magnitudes and distances (see text). Average ratios and error bars are plotted in red.

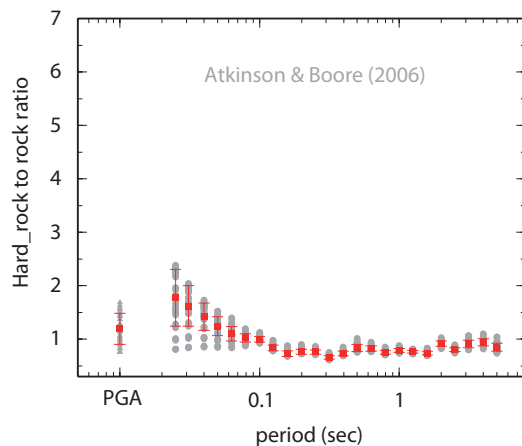


Figure 14: Ratios between hard rock and rock ground motion predictions using Atkinson and Boore (2006) GMPE. Average ratios and error bars are plotted in red.

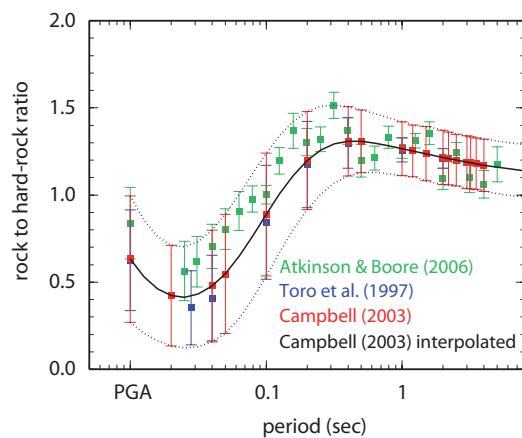


Figure 15: Average rock to very hard rock ratios estimated using: Atkinson and Boore (2006) GMPE (green), Toro *et al.* (1997) GMPE (blue), and Campbell (2003) GMPE (red). The black curve is the interpolation of the ratios computed using Campbell (2003).